

Feed Forward Torque Control: A True Sensorless Control Method for the PM Synchronous Motor and the Hybrid Stepper Motor

Gregory P. Hunter
University of Technology Sydney
greg.hunter@uts.edu.au

Summary--Previous methods of sensorless vector control of the permanent magnet synchronous motor (PMSM) operate by estimating the rotor position from the back EMF or from saliency detection using high frequency injection. This paper introduces an entirely new method of sensorless control of the PMSM where instead of trying to determine the rotor position, a new torque controller structure is developed which uniquely does not need position information, allowing inherent sensorless operation down to zero speed. As a bonus, the new structure uses only low bandwidth current sensing, provides instantaneous torque response (within one sample period) and makes available instantaneous values of speed, position and load torque for use by outer speed and position control loops. Combined with a specifically developed outer speed controller, it allows speed control of high dynamic performance at all speeds including zero with a high tolerance to inertia changes. The new torque control method is called Feed Forward Torque Control. Its operation using a hybrid stepper motor is described.

I. INTRODUCTION

Vector control of AC motors has evolved around a standard control structure for the torque control section. A general block diagram of this structure applied to a permanent magnet synchronous motor (PMSM) is shown in Figure 1. The torque and flux controllers are traditionally implemented using PI control of the d and q axis currents. A variation to this structure is Direct Torque Control (DTC) [1] where the motor torque and flux are directly calculated from the motor voltages and currents and are used instead of the d and q axis currents for feedback control. DTC also uses hysteresis controllers instead of the more traditional PI controllers.

There are many problems with the traditional torque control structure. A major problem is the need for high current loop bandwidth in order to obtain fast torque response. Also, the traditional PI controllers used in the feedback current loops are difficult to implement due to the non-linear nature of the machine equations and to delays in the pulse width modulation process especially as the PWM carrier to output frequency ratio reduces [2]. DTC attempts to overcome these problem by using fast hysteresis control of flux and torque, but at the expense of higher torque ripple and variable switching frequency. More recently, Model Predictive Control (MPC) has been used to improve on DTC by using a more intelligent selection of the switching instances than just straight hysteresis control [3]. DTC and MPC still require very high current sensor bandwidth. MPC also suffers from requiring high computing resources due to its need to analyze many possible future switching scenarios.

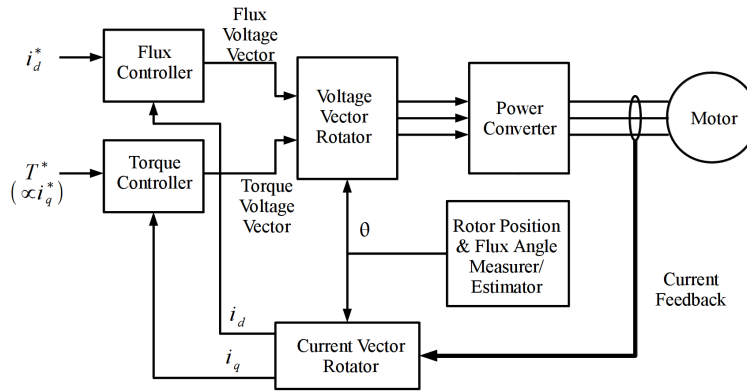


Figure 1. Conventional torque controller for PMSM.

Another problem with the traditional torque control structure is the need to measure or estimate the rotor position. For sensorless control of the motor, the rotor position must be estimated from the motor voltages and currents. For the PMSM this has proved particularly difficult [4]. No universal method which will work with all PMSM types at all speeds has been devised.

For a PMSM with rotor saliency it is possible to determine the rotor angle by directly measuring the spatial inductance variation by injecting high frequency or pulse test currents [5], [6]. For a PMSM without saliency, the only available method of determining the rotor angle is by using an estimation method using the motor's back EMF. Many different estimators of this type have been devised, both for PI current feedback systems [4] and for DTC systems [7]. The problem with these methods is that the back EMF is difficult to measure at very low motor speeds and does not exist at all at zero speed.

This paper presents a new torque controller structure in which torque is controlled by modulating the applied flux vector phase angle via speed modulation rather than by modulating the current amplitude as used in the traditional torque control structure. In this new structure, motor voltages are set using feed forward control rather than by feedback PI current control. The position sensing problem is avoided by, uniquely, eliminating the need to measure the rotor position. Instead, the rotor position is determined indirectly by providing the conditions that force the rotor to lock into the required alignment. At high speeds, the presence of back EMF causes the q axis current to be sensitive to alignment errors and this can be used to force alignment. At low speeds, positive d axis current is applied to lock the rotor into alignment. The new torque controller has fast torque response together with very low torque ripple and requires only low bandwidth current sensing and only modest processor resources. It was first described by the author in a less developed form and without detailed analysis in [8].

Also presented in this paper is a new speed controller specifically tailored to the new torque controller. It has no integrator, operates with no overshoot on step speed changes and remains stable under a wide variation in load inertia.

The new combined torque and speed controller was derived from first principles but has elements in common with existing v/f controllers [9], [10], which also do not require knowledge of the rotor position. It also has some elements in common with feed forward voltage type vector control for induction motors, a method investigated in the early development of vector control [11], [12] and briefly looked at more recently [13], [14]. Not requiring the rotor position, the new structure operates at all speeds including zero without modification. As well as being truly sensorless, it also gives superior motor control performance in many areas compared with the standard torque controller. Features of the new torque and speed controller include:

- 1) Fast dynamic performance at all speeds, including zero.
- 2) Uses fundamental mode. No high frequency injection. Saliency is not required.
- 3) Much lower bandwidth current sensing requirements than existing methods.
- 4) Low demands on the digital signal processor.
- 5) One sample (dead beat) response time to torque commands.
- 6) Insensitive to stator resistance variation, even at zero speed.
- 7) Provides damping to mechanical resonances. No need for anti-resonance filters on the torque command signal.
- 8) Very low torque ripple giving exceptionally smooth speed control and very quiet operation.
- 9) Much lower PWM carrier to output frequency ratios possible compared with PI current controllers.
- 10) Rapid response flux weakening allowing fast dynamic performance in flux weakened regions.
- 11) Does not require voltage head-room for feedback loop operation allowing full utilization of the available supply voltage.
- 12) Precise, immediate values of speed, position and load torque are made available for the outer feedback loops. This allows the the speed and position loops to operate at high bandwidth without integrators and with no overshoot.

The new control method is called Feed Forward Torque Control (FFTC) due to its use of feed forward controllers for both the motor voltages and rotor speed. An overview of the new torque controller structure is provided in Section II. A detailed description of each element in the structure is provided in Sections III-VI. Section VII describes the additions for flux weakening control and Section VIII describes the added speed control loop. Sections IX and X provide dynamic analysis at high and low speeds, Section XI describes the controller implementation and Section XII provides experimental results. Concluding remarks are provided in Section XIII.

II. TORQUE CONTROLLER STRUCTURE

The traditional torque controller structure requires the angular position of the rotor at all speeds. To this end, the rotor position must be provided, or at least estimated. In reality, to control the motor, the rotor position only needs to be able to be controlled, not measured. A common motor controller where this is made use of is the stepper motor controller in which a fixed amplitude rotating stator current is applied to rotate the rotor. Another common method that does not need rotor position information is v/f control, most frequently applied to induction motors but also to PMSM's [10]. These simple methods generally have poor performance and in particular do not have an inner torque controller to allow torque limiting.

FFTC also makes use of the lack of need for rotor position knowledge but uses a different mechanism. Central to FFTC is the addition of a load model to provide rotor position and speed indirectly. The load model calculates the rotor speed and position from the torque command. A second important modification to the traditional torque controller is the replacement of the feedback current controllers with feed forward controllers which compute the motor voltages directly from the command currents. Crucially, this frees up the q axis current feedback allowing it to be used to provide corrections to the load model. The q axis current feedback signal is used first

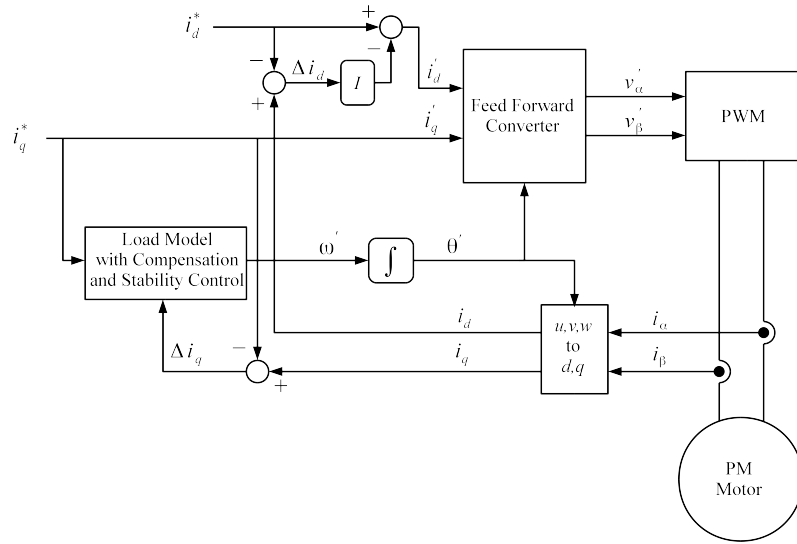


Figure 2. Basic structure of the new torque controller.

to ensure the load model derived speed and position track the actual values and second to provide rotor damping.

The basic structure of the new torque controller is shown in Figure 2 as applied to a 2-phase motor such as the hybrid stepper motor used in experiments described in this paper. The new structure is described as follows, with a star superscript ($*$) used to indicate command values, a tick ($'$) used to indicate applied values and a tilde (\sim) used to indicate estimated values. The equivalent two-phase, two-pole version of the motor is assumed for the description and analysis removing the added complication of considering the pole number.

The q axis current command i_q^* (proportional to torque), which is also the applied q axis current i'_q , together with the applied d axis current i'_d and the applied rotor flux angle θ' are the inputs to the Feed Forward Converter which uses the machine equations to generate the two phase voltages for the Pulse Width Modulator (PWM). This converter is described in Section III and the PWM is described in Section IV.

The applied d axis current i'_d is the command value i_d^* with a correction applied by subtracting a proportion of the integral of the d axis current error Δi_d generated by the integral controller I . This correction operates slowly and is included to reduce the d axis current's sensitivity to errors in the estimated stator resistance and errors in the PWM.

The Load Model with added compensation and stability control is fed by the q axis current command signal i_q^* and generates the applied rotor speed ω' which in turn is integrated to generate the applied rotor electrical angle θ' . For most applications, only the load inertia needs to be modeled, with q axis current error feedback Δi_q used to compensate for extra load torque and errors in the estimate for the inertia. This feedback signal is also used to dampen any motor instability by modulating the applied rotor speed ω' as first proposed in [9].

The Load Model and the following integrator for generating the applied rotor angle replace the rotor position estimator required in the conventional torque controller, overcoming the problem of estimating the rotor position particularly at zero speed. Also to advantage the Load Model and speed integrator provide accurate and immediate values of load torque, speed and position for use in outer speed and position control loops. Details of the Load Model with compensator and stability correction are given in Section V.

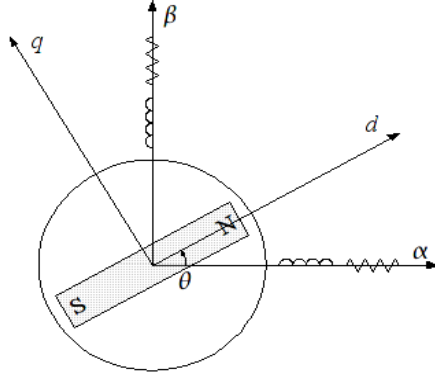


Figure 3. Diagram showing the fixed and rotating axes representations of the two-phase, two-pole equivalent PMSM.

Because the feedback current is used to correct the load model which only involves mechanical time constants, rather than the electrical time constants associated with the traditional feedback torque controller, the required bandwidth of the current feedback signals is greatly reduced as is the influence of current signal noise and harmonics on the output voltage ripple.

One difficulty with the new torque controller structure is that at or near zero speed, the feedback torque current error Δi_q does not respond to static rotor position errors and cannot be used to correct the static applied rotor angle. This is fixed by locking the rotor position to the correct angle by applying a positive d axis current. This prevents the applied and actual rotor angles drifting apart at zero speed without affecting the dynamics of the controller. In this mode, at zero speed, torque control is feed forward with load torque changes having no effect. At higher speeds, feedback torque predominates and the d axis current can be reduced to zero as it is not needed.

III. FEED FORWARD CONVERTER

The Feed Forward Converter block generates the motor voltages from the applied dq axes currents i'_d and i'_q for an applied rotor electrical angle θ' . The outputs of this block are the 2-phase applied output motor voltages v'_α and v'_β for use by the PWM generator. These outputs are generated using the motor equations linking v_α and v_β to i_d and i_q which are derived as follows:

Using the stationary $\alpha\beta$ axes shown in Figure 3, the motor currents and voltages are related by the equation

$$\begin{bmatrix} v_\alpha \\ v_\beta \end{bmatrix} = \begin{bmatrix} R i_\alpha \\ R i_\beta \end{bmatrix} + p \begin{bmatrix} L i_\alpha + \lambda_{r\alpha} \\ L i_\beta + \lambda_{r\beta} \end{bmatrix} \quad (1)$$

where R and L are the stator resistance and inductance, $\lambda_{r\alpha}$ and $\lambda_{r\beta}$ are the flux linkages in the α and β axes from the rotor and p is the differential operator. It is assumed the motor has no saliency and thus the stator inductances do not vary with the rotor angle.

Converting the stationary $\alpha\beta$ frame currents and flux linkages to the rotating dq frame shown in Figure 3 using the general conversion formula:

$$\begin{bmatrix} \alpha \\ \beta \end{bmatrix} = \begin{bmatrix} \cos \theta & -\sin \theta \\ \sin \theta & \cos \theta \end{bmatrix} \begin{bmatrix} d \\ q \end{bmatrix} \quad (2)$$

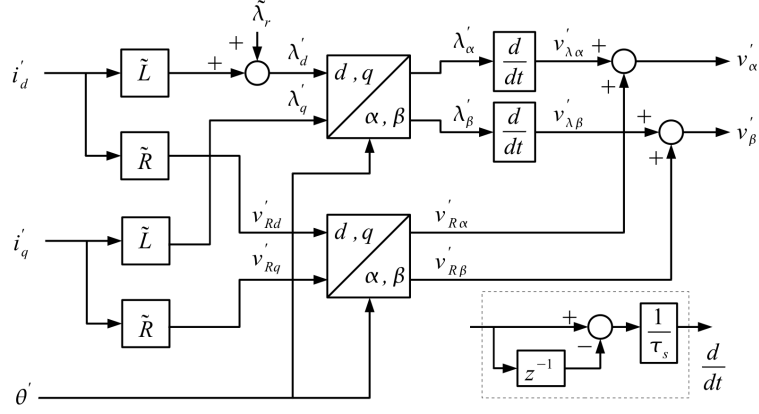


Figure 4. Implementation of equation (3) in the Feed-Forward Converter.

and assuming the rotor flux is aligned on the d axis, giving $\lambda_{rd} = \lambda_r$, the peak rotor flux linkage, and $\lambda_{rq} = 0$, the following equation is obtained:

$$\begin{bmatrix} v_\alpha \\ v_\beta \end{bmatrix} = \begin{bmatrix} \cos \theta & -\sin \theta \\ \sin \theta & \cos \theta \end{bmatrix} \begin{bmatrix} R i_d \\ R i_q \end{bmatrix} + p \begin{bmatrix} \cos \theta & -\sin \theta \\ \sin \theta & \cos \theta \end{bmatrix} \begin{bmatrix} L i_d + \lambda_r \\ L i_q \end{bmatrix} \quad (3)$$

This is the equation implemented in the Feed Forward Converter.

Note that equation (3) can be expanded further to the following familiar motor voltage equations in the dq frame:

$$\begin{bmatrix} v_d \\ v_q \end{bmatrix} = \begin{bmatrix} R + Lp & -\omega L \\ \omega L & R + Lp \end{bmatrix} \begin{bmatrix} i_d \\ i_q \end{bmatrix} + \omega \lambda_r \begin{bmatrix} 0 \\ 1 \end{bmatrix} \quad (4)$$

by putting:

$$\begin{bmatrix} v_\alpha \\ v_\beta \end{bmatrix} = \begin{bmatrix} \cos \theta & -\sin \theta \\ \sin \theta & \cos \theta \end{bmatrix} \begin{bmatrix} v_d \\ v_q \end{bmatrix} \quad (5)$$

followed by expanding the differentials and some careful algebraic manipulation.

A block diagram of the implementation of equation (3) using estimated values of the motor parameters is shown in Figure 4. Variables v'_{Rd} , v'_{Rq} , $v'_{R\alpha}$ and $v'_{R\beta}$ are the calculated IR voltage drops in the dq and $\alpha\beta$ axis.

As shown in the inset, in the z domain, the derivative is handled by subtracting the previous sample value of the flux in the stationary frame from the present sample value then scaling by the inverse of the sample period τ_s .

The L/R time constant in the Feed Forward converter can cause excessively long settling times to load changes if it is too large. This is corrected by adding extra artificial resistance to the inverter outputs using feedback and increasing \tilde{R} to match the extra artificial resistance, reducing the L/R time constant to a suitable value. The selection of this extra resistance is discussed in Section X.

For a DSP implementation, the sample period for calculations is normally set to half the PWM carrier period. The dq to $\alpha\beta$ conversion block is usually implemented using sine and cosine look-up tables.

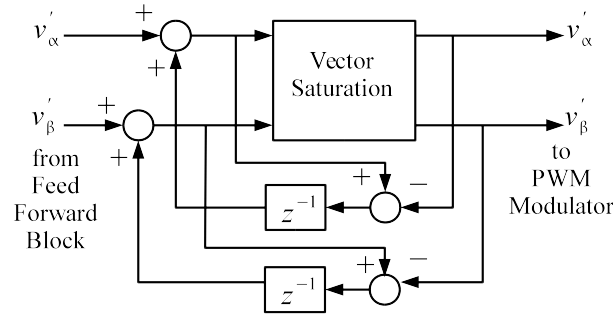


Figure 5. Method of pulse clipping and lengthening.

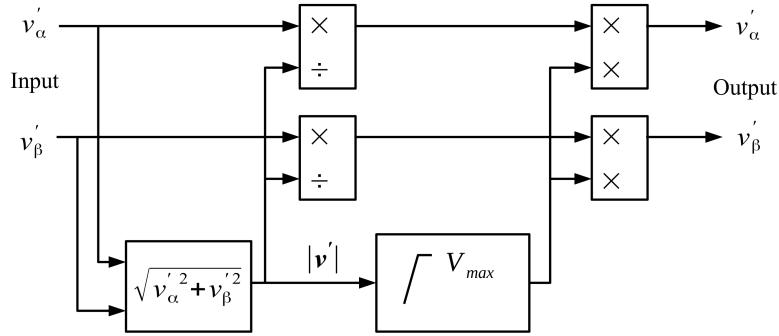


Figure 6. Vector saturation method.

An advantage of using the direct implementation of equation (3) is that the sine and cosine look-up tables for the dq to $\alpha\beta$ conversion block for the flux linkages do not need to be very accurate because an error in one sample value will cause a short term proportional current error only ($L\Delta i = \Delta\lambda$) which would be considerably less than the carrier induced current ripple anyway. Contrast this to the normal scheme using equations (4) and (5) where the vector rotation acts on the voltages instead of the flux linkages. The sine and cosine look-up tables would then need to be very accurate because an error in one sample value would cause a permanent step change in current ($L\Delta i = \int \Delta v dt$).

Also, a part of the feed forward implementation scheme of equation (3) and Figure 4 is the direct voltage to voltage vector rotation of the estimated motor IR drop voltages. Since these added voltages compensate only for the motor resistance voltage drops, the look-up tables for the dq to $\alpha\beta$ conversion also do not need to be very accurate.

Another advantage of using the direct implementation of equation (3) is that because the output voltages v'_α and v'_β are the changes in the flux linkages over each sample period, these voltages are equal to the average expected voltages over the period ($\Delta\lambda = \Delta \int v dt$). The resulting PWM pulse widths are thus proportional to the average output voltages over the period. It has been shown [15] that this greatly reduces subharmonic currents when the carrier to output frequency ratio is low allowing much lower ratios to be used. It is possible to suppress subharmonics even further by using a double integral modulation scheme [16].

For large changes between successive sampled values of the applied flux linkages λ'_α and λ'_β caused, for instance, by a step change in the torque command, the output sampled value of each differentiation block could be large enough to cause clipping in the PWM output voltage. This

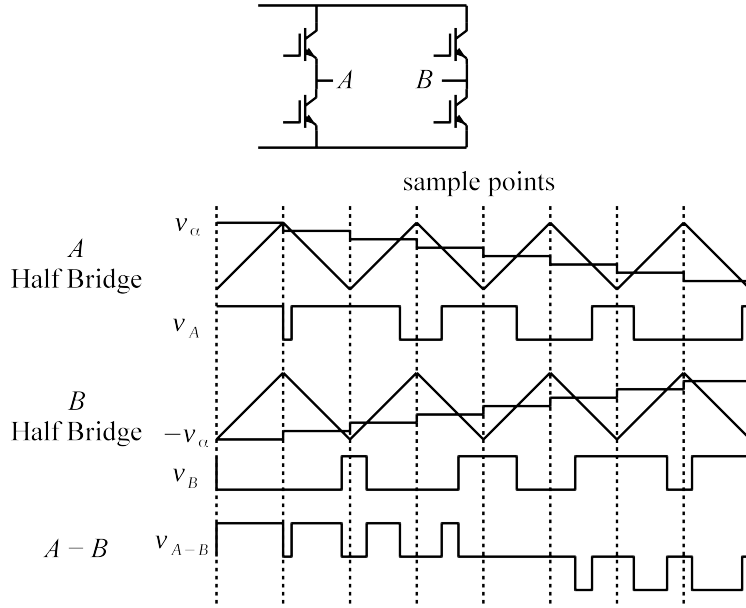


Figure 7. Method of generating the PWM outputs for the α phase.

would result in the needed change in flux linkage and the corresponding change in current not appearing on the motor. To prevent this happening, a pulse lengthening unit is added before the PWM modulator as part of the Feed Forward Converter to limit the peak voltage input without changing the voltage integral. A simple method that can be used to implement the required pulse lengthening is shown in Figure 5. This pulse lengthening and clipping unit modifies the applied output stationary axis voltages v'_α and v'_β by clipping their vector magnitude and adding the resultant errors to the inputs at the next sample.

The Vector Saturation unit clips the $[v'_\alpha, v'_\beta]$ vector to a fixed magnitude so it is limited to a circle in the space vector plane. A simple method of implementing clipping to a circle which avoids calculating the vector angle is shown in Figure 6. The vector components are normalized by dividing by the vector magnitude then rescaled using the clipped value of the magnitude. For a two-phase double-bridge inverter driving a stepper motor as used in the experiment for this paper, the vector magnitude should be clipped to $V_{max} = V_{DC}$.

IV. PULSE WIDTH MODULATOR

For a full bridge PWM inverter on each output phase as is normally used for a two phase motor, there are many possible modulation schemes. For the experiments used for this paper, double edge modulation of each half bridge using triangular carrier comparison is used. The scheme is illustrated in Figure 7 for the α phase. A triangular carrier wave of half the sample frequency is compared with the desired output v'_α to generate the output for the A half bridge and with $-v'_\alpha$ for the B half bridge. This scheme minimizes switching losses as only one half bridge switches at each change in output state and the switching losses are shared equally amongst the four output transistors.

V. LOAD MODEL AND COMPENSATOR

A block diagram of the Load Model with i_q compensation and damping control is shown in Figure 8. The Load Model is an inertial model with transfer function $\lambda_r / \tilde{J} s$ where \tilde{J} is an estimate of

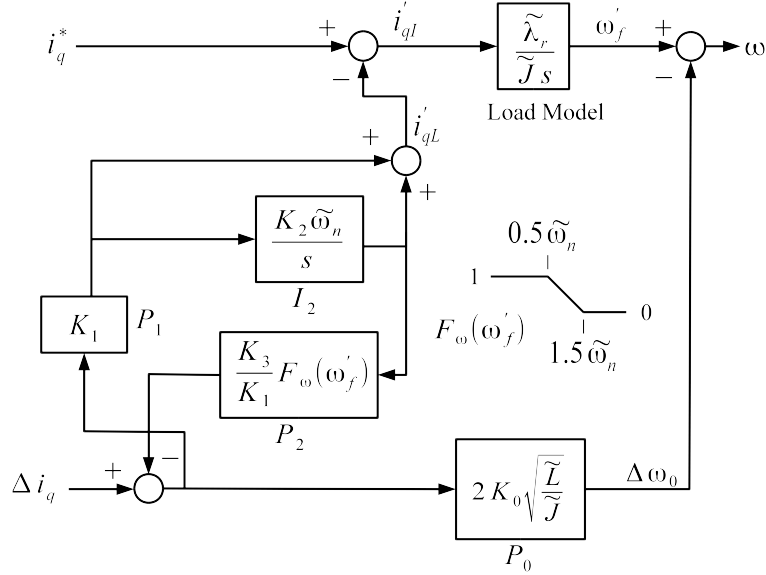


Figure 8. Load model with compensation.

the 2-pole equivalent inertia (actual inertia divided by the square of the number of pole pairs), the output of which is the speed ω'_f which can be considered as the filtered version of the applied output speed ω' . The difference is the addition of the output of the stability correction block P_0 . Like traditional PMSM v/f controllers [10] this controller requires a proportion of the torque current error Δi_q to be subtracted from the speed to stabilize the drive to prevent hunting. The required correction speed $\Delta\omega$ is given by [10]:

$$\Delta\omega = 2\zeta\sqrt{\frac{L}{J}}\Delta i_q \quad (6)$$

where ζ is the damping factor, typically set to 1 for critical damping. The required damping is provided by gain block P_0 with gain set by equation (6) with constant K_0 set to the damping factor and using estimates of L and J and with output speed correction $\Delta\omega_0$.

Before being applied to the load model, the command torque current i_q^* is corrected by subtracting the applied load torque current i'_{ql} . Ignoring for now block P_2 which takes effect at low speed, this load torque current is found from a proportional-integral controller, blocks P_1 and I_2 in Figure 8, with the torque current error Δi_q as its input. Any change in actual load torque will cause a torque current error to occur which will then be corrected by the PI controller. In this way, the applied load torque current tracks the real load torque current.

The use of a PI controller is possible because, as will be shown in Section IX, the response of the error current Δi_q to a change in the applied rotation speed ω' is linear and independent of the motor speed. This characteristic allows the torque controller to operate at all speeds including zero with the same dynamic response. This provides the controller with a major advantage over existing torque controllers which must work with non-linear transfer functions.

To choose the controller gains, a dynamic response analysis is required, which is undertaken in Section IX. Briefly, it is necessary to recognize that this torque PI controller acts with the stabilizing branch P_0 to form a second order P+I+I² controller. The corresponding normalized gain constants are K_0 , K_1 and K_2 as shown in Figure 8. The normalization scaling shown is chosen to make the gain constants machine independent. Note that the scaling shown in the earlier paper on

FFTC [8] for K_0 was in error. For the gain constant of the I_2 integrator block, the scaling includes an estimated value of the natural frequency ω_n . This is the hunting frequency of the motor when operating under undamped open loop voltage control at high speed and is given by $\omega_n = \lambda_r / \sqrt{LJ}$ [10]. Constant K_0 which as previously shown is the damping factor is typically set to 1. Constants K_1 and K_2 are typically set to 0.5 for optimum response characteristics.

To prevent the output of integrator I_2 drifting at zero speed when Δi_q does not respond to changes in the load torque, the integrator is turned into a low pass filter by adding a feedback path around it, shown as block P_2 in Figure 8. This path is only needed at or near zero speed so its gain is reduced as speed is increased by including the function $F_\omega(\omega'_f)$. This function is set to 1 at zero speed reducing to zero at higher speeds. The input parameter used for this function is the filtered version ω'_f of the applied speed obtained before the proportional term is added. From empirical tests, a suitable choice for this function is as shown in Figure 8. This is a simple ramp function staying at 1 up to $\omega'_f = 0.5\tilde{\omega}_n$ then ramping to zero at $\omega'_f = 1.5\tilde{\omega}_n$.

The output of P_2 is subtracted from the torque current error Δi_q rather than the input of the integrator I_2 in order to keep the average value of $\Delta\omega_0$ zero, necessary to ensure there is no offset in the filtered speed ω'_f which is used in the outer speed control loop.

The DC gain of the integrator at zero speed is the inverse of the gain constant K_3 . The choice for K_3 depends on the application. When the motor is brought to zero speed, the value stored on the output of the integrator I_2 is the stored load torque from when the motor speed was high enough for the load torque to be measurable, which is when the motor back EMF is high enough to drive a large change in Δi_q when the motor flux phase angle differs from the applied phase θ' . When zero speed is reached, this value slowly returns to zero at a rate depending on the value of K_3 . At the same time, the rotor angle settles to an offset value from the applied angle depending on the standstill load torque and the level of d axis current i_d that has been applied to hold the rotor in position. For a fixed load torque where the speed is changed slowly through zero, a low value for K_3 is preferred, perhaps 0.1 or less. For a position controller where settling time at zero speed should be as fast as possible, a high value for K_3 is called for, perhaps as high as 1.0. A compromise value which works well for most applications is 0.25.

VI. D AXIS CURRENT CONTROL

As mentioned in Section II and shown in Figure 2 the i_d controller uses feed forward control with added feedback compensation. The feedback corrects for any steady state errors in i_d caused by errors such as the estimation of parameters in the Feed Forward Converter. The feedback compensator uses a simple integral controller where the integral of the current error is subtracted from the reference current. The integral gain is set to $K_1\tilde{\omega}_n$ to match the effective gain of the integral controller in the q axis load model compensator.

As stated in Section II, at start up the d axis reference current must be set high enough to provide a holding torque greater than and preferably twice the difference between the load model torque and the actual torque. For example, if there is a start up 2-pole equivalent friction torque T_F then the d axis reference current i_d^* at start up must be set to greater than T_F/λ_r . As the motor speed rises and the rising back EMF allows the q axis current feedback loop to react to load torque errors, i_d^* can be reduced. In the simulations and experiments described in this paper, i_d^* is reduced as the speed rises by a simple two stage ramp function $F_d(\omega')$ which can be set to the same function as used for the load compensator, $F_\omega(\omega'_f)$.

If V_M is the set maximum output voltage during flux weakening, the d flux reference λ'_{df} must be chosen so that:

$$\sqrt{v_q'^2 + v_d'^2} = V_M \quad (9)$$

V_M should be set slightly lower than the maximum available voltage to allow some voltage overhead to handle transient components. Experience has shown that setting V_M to 95% of maximum allows ample headroom. It can be set to 100% if slight errors in the applied position angle θ' during transients is acceptable. In this case it would also be wise to disable the pulse lengthening of Figure 5 during flux weakening.

In an actual implementation, voltages would be normalized to the modulation index for exact control of the output voltage headroom as a proportion of the maximum available output voltage.

In equation (8) flux linkage λ'_d is dependent on v'_q which when operating at maximum voltage V_M is from equation (9):

$$v'_q = \text{sign}(\omega') \sqrt{V_M^2 - v_d'^2} \quad (10)$$

Using equation (8), the flux linkage reference is given by:

$$\begin{aligned} \lambda_{df}^* &= \frac{1}{\omega'} (v'_q - v'_{Rq}) \\ &= \frac{1}{\omega'} [\text{sign}(\omega') V_M \sqrt{1 - \left(\frac{v'_d}{V_M}\right)^2} - v'_{Rq}] \\ &= \frac{1}{|\omega'|} [V_M \sqrt{1 - \left(\frac{v'_d}{V_M}\right)^2} - \text{sign}(\omega') v'_{Rq}] \end{aligned} \quad (11)$$

An inspection of equation (11) shows that v'_d/V_M must be kept less than one. The applied d axis voltage v'_d depends on the applied torque so it can be limited in magnitude by controlling the q axis torque current limits as follows:

The q axis applied flux linkage and current are related by the equation

$$\lambda'_q = i'_q \tilde{L} \quad (12)$$

where \tilde{L} is the estimated motor inductance.

Using this relation in equation (7) to find i'_q :

$$i'_q = -\frac{1}{\tilde{L}\omega'} (v'_d - v'_{Rd}) \quad (13)$$

The absolute maximum value of v'_d is limited to V_{DM} which must be less than V_M to ensure v'_d/V_M is less than 1. In an actual implementation, V_{DM} would typically be set to 80% of V_M . This leaves enough voltage margin for flux weakening to operate. To maximize available torque, values as high as 90% have been successfully tried.

From equation (7) for positive speed and positive torque voltage v'_d is negative. It must be limited to $-V_{DM}$. This sets the maximum limit of i'_q to:

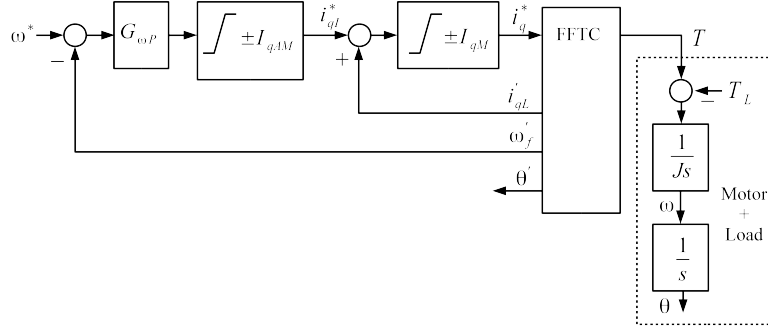


Figure 10. Speed control loop.

$$i'_{qmax} = \frac{1}{\tilde{L}\omega'} (V_{DM} + v'_{Rd}) \quad \text{for } \omega' > 0 \quad (14)$$

For positive speed and negative torque v'_d is positive. This voltage must be limited to V_{DM} restricting the negative limit of i'_q to:

$$i'_{qmin} = -\frac{1}{\tilde{L}\omega'} (V_{DM} - v'_{Rd}) \quad \text{for } \omega' > 0 \quad (15)$$

For negative speed and negative torque, v'_d is negative. It must be limited to $-V_{DM}$ restricting the negative limit of i'_q to:

$$i'_{qmin} = \frac{1}{\tilde{L}\omega'} (V_{DM} + v'_{Rd}) \quad \text{for } \omega' < 0 \quad (16)$$

Finally, for negative speed and positive torque v'_d is positive. It must be limited to V_{DM} restricting the positive limit of i'_q to:

$$i'_{qmax} = -\frac{1}{\tilde{L}\omega'} (V_{DM} - v'_{Rd}) \quad \text{for } \omega' < 0 \quad (17)$$

From the above it can be seen that the equations for i'_{qmax} and i'_{qmin} are swapped depending on the motor rotational direction.

For practical implementation, the above four equations can be combined to create the following continuous torque limits:

$$i'_{qmax} = \frac{1}{|\omega'| \tilde{L}} (V_{DM} + \text{sign}(\omega') v'_{Rd}) \quad (18)$$

$$i'_{qmin} = \frac{1}{|\omega'| \tilde{L}} (-V_{DM} + \text{sign}(\omega') v'_{Rd}) \quad (19)$$

These limits can then be applied to the input command i'_q on top of the normal torque current limits. They should be disabled at zero speed to avoid division by zero.

VIII. SPEED CONTROL LOOP

The block diagram of the speed control loop is shown in Figure 10. Unique to FFTC, advantage is taken of the availability of the applied load torque current i'_{qL} to eliminate the integrator normally used to correct for an offset torque. As well as removing integrator wind-up problems, this results in stable operation without re-tuning for wide changes in inertia although the degree of damping will vary depending on the inertia mismatch.

The speed command input ω^* is compared to the filtered applied speed ω'_f . The error signal passes through a proportional compensator of gain $G_{\omega P}$ to create the command inertial torque current i^*_{ql} . This is limited to plus and minus the maximum acceleration current I_{qAM} . The applied load torque current is then added to create the command torque current i^*_q . A maximum limit of $\pm I_{qM}$, which includes the limits set by equations (18) and (19), is applied to i^*_q as shown to provide torque limiting for the motor.

From inspection of the load model and compensator in Figure 8, when not in torque limit, i^*_{ql} is exactly equal to the input torque current to the load model i'_{ql} . Since the load model used is an inertial model with transfer function $\tilde{\lambda}_r/\tilde{J}s$, i^*_{ql} is exactly the motor acceleration rate times $\tilde{J}/\tilde{\lambda}_r$. The limit $\pm I_{qAM}$ on i^*_{ql} is set to $\pm A_M \tilde{J}/\tilde{\lambda}_r$ setting the maximum acceleration precisely to A_M .

Also from Figure 8, it can be seen that the filtered speed used for feedback, ω'_f , comes straight from the output of the inertial load model. This places the whole speed control loop locally within the controller, allowing any gain value to be used for $G_{\omega P}$ limited only by the sampling rate of the controller. This makes tuning of the speed loop very easy and allows very fast speed responses to be set. It also results in extremely smooth and accurate speed control.

For convenience, the speed loop compensator gain can be normalized to:

$$G_{\omega P} = K_{\omega 0} \tilde{\omega}_n \tilde{J} / \tilde{\lambda}_r \quad (20)$$

The normalized gain $K_{\omega 0}$ can then be set independently of the motor and load parameters. Experience has shown a value for $K_{\omega 0}$ of 1.0 suits most situations.

Because of the ready availability of the rotor position from the torque controller, a position controller can be easily added around the speed controller to produce a high speed sensorless position controller for the motor. A suitable position controller was tried with excellent results but its description is beyond the scope of this paper.

IX. HIGH SPEED DYNAMIC ANALYSIS

There are many ways of analyzing a controller to determine response and stability. Common methods are root locus analysis, Bode plots and the Nyquist stability criterion. Here the more unusual method is used of representing the controller with equivalent electrical circuits. This gives a clearer picture of the controller stability and response when third and higher order systems are being analyzed as is the case here.

To see how the choice of gain constants affects motor response it is necessary to separately analyze the motor response at motor speeds above and below the natural frequency ω_n . The mechanisms for these two situations are quite different but the resulting responses are similar and combine to give the same linear response over the entire speed range. It is also necessary to consider separately the cases when the controller is operating in torque control mode and in speed control mode. This section investigates the response at motor speeds well above ω_n . The case when the controller is in torque control mode is considered first.

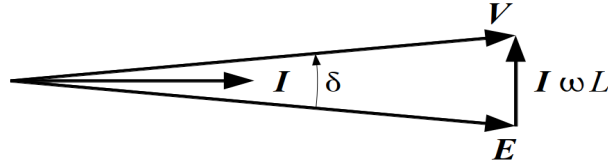


Figure 11. Phasor diagram for rotor retarded by angle δ .

At high speed well above ω_n , for small perturbations, the q axis torque producing current i_q can be assumed to be sensitive to changes in the rotor angle only and can be analyzed most simply using phasor diagrams.

Consider the case of a two pole PMSM operating without load at a high fixed stator frequency ω and with the rotor EMF vector E equal to the applied voltage vector V . Now consider the case of a small perturbation of δ radians in the rotor angle due to instability causing a current I to flow. Ignoring motor resistance, which at high speed would normally be much less than the motor reactance ωL anyway, the phasor diagram shown in Figure 11 applies.

For a small value of δ , $|I|$ is equal to i_q and with $|E| = \lambda_r \omega$ the resulting current is given by:

$$i_q = \frac{\lambda_r \delta}{L} \quad (21)$$

The resulting restoring torque ΔT is given by:

$$\begin{aligned} \Delta T &= \lambda_r i_q \\ &= \frac{\lambda_r^2 \delta}{L} \end{aligned} \quad (22)$$

This causes the rotor speed to change to reduce δ , restrained by the inertia J . The equation of motion is:

$$\begin{aligned} \Delta T &= -J \frac{d\omega}{dt} \\ &= -J \frac{d^2 \delta}{dt^2} \end{aligned} \quad (23)$$

For the analysis, the effect of a change in the controller speed $\Delta \omega'$ driving term can be added to equation (23) as follows:

$$\Delta T = -J \frac{d^2 \delta}{dt^2} + J \frac{d \Delta \omega'}{dt} \quad (24)$$

Replacing δ with ΔT as the independent variable using equation (22) and rearranging:

$$\frac{\Delta T}{J} = -\frac{L}{\lambda_r^2} \frac{d^2 \Delta T}{dt^2} + \frac{d \Delta \omega'}{dt} \quad (25)$$

Integrating this assuming zero initial conditions:

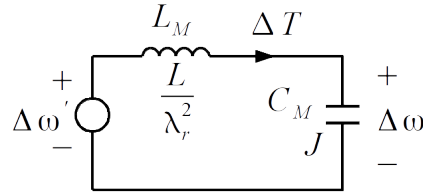


Figure 12. High speed quasi-steady-state mechanical equivalent circuit.

$$\frac{1}{J} \int \Delta T dt = -\frac{L}{\lambda_r^2} \frac{d \Delta T}{dt} + \Delta \omega' \quad (26)$$

It can be seen from this integration that equation (25) can be represented by the mechanical equivalent electrical circuit shown in Figure 12 where $L_M = L/\lambda_r^2$ and $C_M = J$ are the mechanical equivalent inductance and capacitance values (inverse of torsional spring constant and moment of inertia). The resonant frequency of this circuit is the natural frequency ω_n . The voltage across C_M represents the change in rotor speed $\Delta\omega$.

The compensator of Figure 8 controls the damping of this circuit via control of ω' . It should have its gain constants chosen to obtain adequate damping at the highest possible gain. Ignoring for now the integral block I_2 and its feedback block P_3 which are adjusted to have only a minor effect on the response characteristics, the effect of the compensator can be incorporated into the high speed equivalent circuit. This will aid in determining the values of constants K_0 and K_1 .

Assuming no change in the command torque input, the transfer function of the compensator for a change in the applied speed from a change in the q axis current is given by:

$$\Delta \omega' = \frac{K_1 \tilde{\lambda}_r}{\tilde{J}_S} \Delta i_q - 2 K_0 \sqrt{\frac{\tilde{L}}{\tilde{J}}} \Delta i_q \quad (27)$$

When added to the high speed equivalent circuit, the two terms of equation (27) become a mechanical equivalent capacitor and resistor (inertia and inverse of friction). These components and their values are shown in the expanded equivalent circuit of Figure 13.

This equivalent circuit allows easy selection of gain constants K_0 and K_1 . Suitable settings for most applications are $K_0=1$ setting R_{1M} for critical damping of the series $R_{1M}-L_M-C_M$ circuit and $K_1=0.5$ making C_{1M} twice C_M which is high enough to not interfere too much with circuit damping. These values provide a good compromise between compensator gain and damping.

The gain constant K_2 of the second order integral I_2 in Figure 8 is set to as high as possible without interfering too much with the response characteristic provided by the PI compensator. A value of $K_2=0.5$ was found by experiment to be the best compromise.

Of interest is the effect of a change in the torque command T^* , which is the torque command current times the rotor flux $i_q^* \times \lambda_r$, on the equivalent circuit of Figure 13. This is shown in Figure 14. The torque injection shown on the left is the effect of a change in the torque current input i_q^* shown in Figure 8. The torque injection shown on the right is the effect of the Feed Forward Converter changing the motor current as a result of a change in i_q^* , assuming the feed forward motor parameters match the actual motor parameters. A change in the command torque has an immediate effect on the motor torque without exciting the equivalent tuned circuit. Note that any

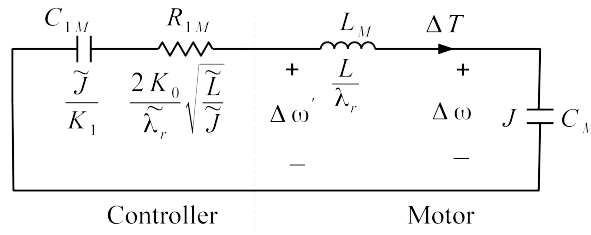


Figure 13. High speed equivalent circuit of controller and motor for stability analysis.

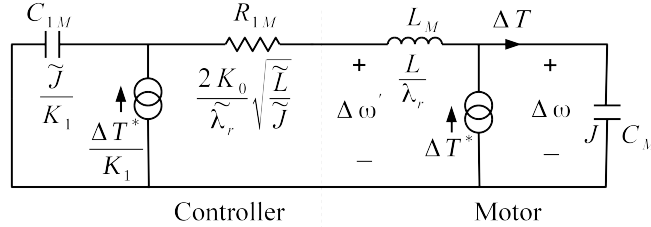


Figure 14. High speed equivalent circuit showing the effect of a change in command torque.

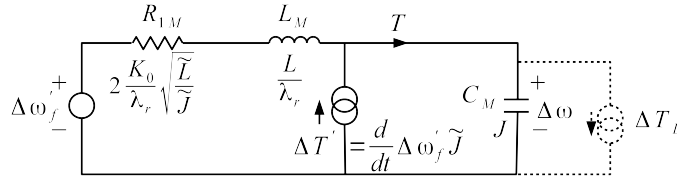


Figure 15. High speed equivalent circuit in speed control mode.

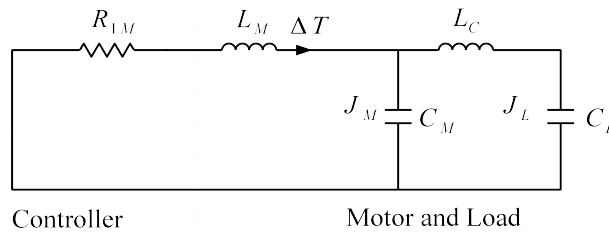


Figure 16. System equivalent circuit of damping for a compliantly coupled load.

parameter mismatch will result in an effective load torque disturbance resulting in the same damped oscillation response. This makes the controller fairly robust to parameter errors.

Now consider the case when the controller is operating in speed control mode. The local speed control loop gives direct control of the filtered speed ω'_f bypassing the torque PI compensator. The resulting controller and motor equivalent circuit is shown in Figure 15 to a first approximation. Shown dotted is the effect of a load torque change ΔT_L . Also shown in this figure is the effect of a change in ω'_f . A change in ω'_f is accompanied with a torque current pulse with a resulting torque pulse $\Delta T'$ which causes the rotor speed to exactly follow ω'_f provided the estimated motor parameters are correct. Again, the effect of the integral block I_2 is ignored for this analysis. Its effect is to speed up the response and reduce damping slightly.

It is of interest to investigate the effect the controller has on a load connected with a high compliance coupling causing a low frequency mechanical resonance. In a conventional controller

the command torque signal must be filtered to avoid exciting this resonance. The effect of adding a two-mass coupled load on the new controller can be seen by adding the load's equivalent mechanical circuit to the high speed equivalent circuit. This extension is shown in Figure 16. Capacitances C_M and C_L are the mechanical equivalent of the motor and load inertias and inductance L_C is equivalent coupling compliance. This circuit shows that by adjustment of the controller gains, particularly K_0 , it should be possible to provide at least partial damping of the load coupling resonance, which is usually sufficient to stop oscillations.

X. LOW AND ZERO SPEED DYNAMIC ANALYSIS

At speeds much less than ω_n and particularly at standstill Δi_q is no longer sensitive directly to changes in the applied speed $\Delta\omega'$ but instead is sensitive to q axis voltage changes. This requires for stability analysis an equivalent circuit that models the electrical characteristics of the motor rather than the mechanical characteristics as used for the high speed analysis.

At zero speed, the rotor is kept in position by the application of a positive d axis current but the dynamics are determined by the q axis external impedance imposed by the inverter. To analyze the dynamics, the q axis equivalent circuit of the motor needs to be derived. This will now be derived using an intuitive method that looks at the motor resonances. A more analytic but less intuitive derivation using the motor equations is also possible.

Consider a two-phase, two-pole PMSM with no external load except the load inertia and with a quasi-stationary rotor with the controller d and q axes aligned with the two windings. Assume a fixed current I_d in the winding aligned with the d axis locking the rotor to this axis. Now consider the equivalent electrical LC circuit for the stationary q axis for an undamped oscillating rotor with the q axis winding open circuit. The equivalent LC tuned circuit is shown in Figure 17. The equivalent parallel inductance is L_p and the equivalent capacitance is C_p .

Now consider when the rotor is off the d axis current alignment by a small angle δ during unstable oscillation. The resulting restoring torque is $I_d \lambda_r \sin \delta$ or $I_d \lambda_r \delta$ to a first approximation. The equation of motion of the rotor is:

$$J \frac{d^2 \delta}{dt^2} = -I_d \lambda_r \delta \quad (28)$$

For electrical circuit equivalence, this must match the differential equation for the equivalent tuned circuit with circulating current i_p which is:

$$C_p \frac{d^2 i_p}{dt^2} = -\frac{1}{L_p} i_p \quad (29)$$

The tuned circuit component values can be found by matching terminal voltage, energy and resonant frequency. The q axis terminal voltage is $\lambda_r d \delta / dt$ which in the equivalent circuit is the voltage on the capacitor giving the energy stored in the capacitor as $0.5 C_p (\lambda_r d \delta / dt)^2$. This is the kinetic energy $0.5 J (d \delta / dt)^2$ giving:

$$C_p = \frac{J}{\lambda_r^2} \quad (30)$$

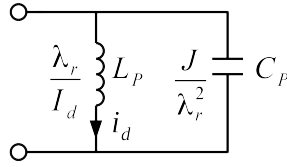


Figure 17. Quasi-stationary open circuit q axis equivalent circuit with fixed d axis current.

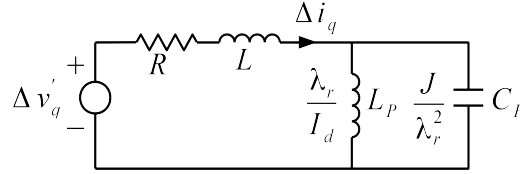


Figure 18. Complete q axis quasi-steady state equivalent circuit of the motor at zero speed.

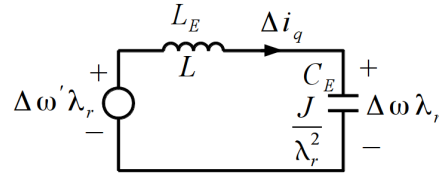


Figure 19. High speed quasi-steady-state equivalent circuit transformed to electrical quantities..

Matching the inverse square of the resonant frequencies gives $L_p C_p = J / (I_d \lambda_r)$ giving a value for the inductor of:

$$L_p = \frac{\lambda_r}{I_d} \quad (31)$$

Finally, equating the capacitor voltage $\lambda_r d\delta/dt$ to the inductor voltage $L_p di_p/dt$, the rotor deviation angle is found to be:

$$\delta = \frac{i_p}{I_d} \quad (32)$$

To complete the q axis equivalent circuit for quasi-stationary rotor oscillations, the winding inductance and resistance can be added as shown in Figure 18. Also added to this circuit is the q axis excitation voltage deviation $\Delta v'_q$ from the controller. This circuit model was derived for a stationary motor with no load but it also holds for low speed operation. $\Delta v'_q$ is controlled by the Feed Forward Converter block which connects it to changes in the applied speed according to the equation:

$$\Delta v'_q = \Delta \omega' \tilde{\lambda}_r \quad (33)$$

To compare this circuit to the mechanical high speed equivalent circuit of Figure 12, the variables used in Figure 12 can be changed from a change in torque to the equivalent change in q axis current

$\Delta i_q = \Delta T / \lambda_r$, and from a change in rotational speed to the equivalent back EMF $\Delta \omega \lambda_r$. The resulting new high speed equivalent circuit with transformed component values is shown in Figure 19. Note that, not unexpectedly, the capacitance value is the same as that of the low speed q axis equivalent circuit.

Comparing the motor response circuit of Figure 19 to Figure 18 and using equation (33) from the Feed Forward Converter, the response of Δi_q to $\Delta \omega'$ is similar except for the secondary influence of L_p . Importantly, the similar linear high frequency response of the two circuits allows the use of a linear feedback compensator as described in Section V for the entire speed range.

So far in the analysis it has been assumed that the angle of the d axis current vector is fixed in the stationary frame. It can be seen in Figure 2 and Figure 8 that transients at zero speed also cause transients in the applied speed and thus also in the applied vector angle used in the Feed Forward Converter. This adds an extra degree of damping not considered so far which will now be investigated.

A special case to be considered for the dynamic response is the effect of a step torque disturbance applied at zero speed when in speed control mode. A load torque at zero speed results in a rotor angle offset the amount of which depends on the torque and the level of d axis holding current. Ideally when the torque is changed, the rotor offset angle should settle to its new value as quickly as possible with minimal overshoot.

With a torque disturbance at zero speed, the resulting sudden movement of the rotor produces a back EMF which in turn causes a pulse of current in the q axis the amplitude of which depends on the combined impedance of the stator and the controller. The resistance component of this impedance provides damping. Another effect, due to the Feed Forward Converter also controlling the d axis current vector, is that the pulse of q axis current results in a change in the applied speed $\Delta \omega'$ which in turn moves the applied angle of the d axis current vector. This dragging of the d axis current vector provides extra damping. The combined effect of these two damping mechanisms are shown in the equivalent electrical circuit of Figure 20. It is assumed in this circuit that only the proportional block P_0 of the compensation network shown in Figure 8 is significant and the rotor offset angle δ is small enough so that $\delta \approx \sin \delta$.

The added voltage source V_p shows the effect of the change in applied speed on the Feed-Forward Converter due to the change in q axis current. The voltage across C_p is the back EMF generated by the rotor movement from the torque disturbance. The voltage source V_p is the countering applied back EMF generated by the applied speed change $\Delta \omega'$ acting on the Feed-Forward Converter. Because this also rotates the d axis current vector, affecting the resultant torque generated by the rotor offset, it appears inside the $L_p C_p$ tuned circuit.

To provide damping, the controller is modified to artificially add a resistive component R_E to the inverter output impedance. This is set to $K_R R_n - R$ where $R_n = \lambda_r \sqrt{L/J}$ is defined as the natural resistance and K_R is a dimensionless tuning constant. The changes to the controller required to create this resistive component on the output can be seen in the full controller block diagram of Figure 22. This changes the effective motor stator resistance from R to $K_R R_n$. This is also used as the motor resistance in the Feed Forward Converter calculations.

Constant K_R sets the damping for a zero speed torque disturbance. Simulations show the optimum value is about 1 for any motor type and any setting of the d axis holding current. Figure 21 shows the response of the rotor angle offset to a small torque change using the motor parameters of Tables I and II with $K_R = 1$. The responses using the equivalent circuit of Fig 20 and a full simulation using the Matlab/Simulink program for d axis currents of 0.5 and 1.5 A are shown. The larger error

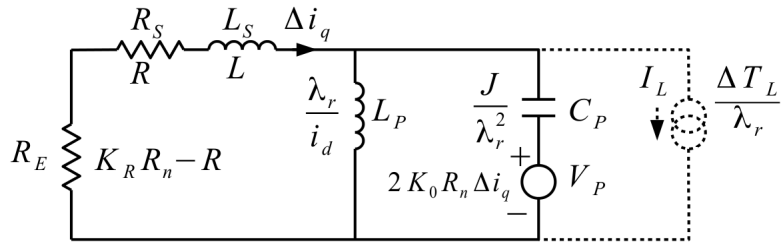


Figure 20. Zero speed equivalent circuit for a torque disturbance.

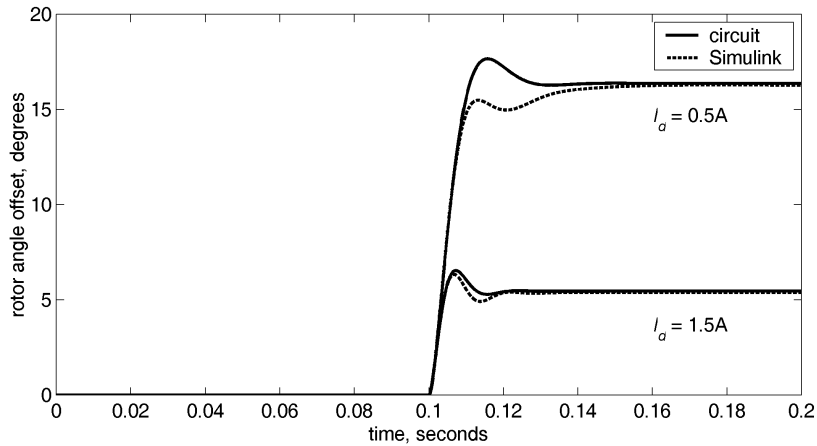


Figure 21. Rotor angle offset response to a step torque disturbance at zero speed for the equivalent circuit and the full simulation.

in the response for $I_d = 0.5A$ is probably due to the increased error in the approximation of $\sin \delta$ to δ in radians.

XI. IMPLEMENTATION

The complete controller in block diagram form suitable for practical implementation is shown in Figure 22. This is used for both simulations and experiments. Before undergoing dq to $\alpha\beta$ coordinate transformation, the applied stator flux linkages and the applied stator IR voltages are normalized to the modulation index by dividing by the maximum PWM output voltage before saturation, V_{max} , which is updated continuously from a reading of the DC link voltage in an actual system. Variables normalized in this way are indicated in Figure 22 by a hat (^) symbol. Single sample delays where calculations stop in one sample and start in the next sample are shown in the diagram with the z domain representation z^{-1} .

Shown is the detailed mechanism for generating the d and q error current values Δi_d and Δi_q . A delay is shown added to the d and q reference currents and to the sine and cos values of the applied rotor angle to compensate for the delay in the PWM modulator. If significant filtering is used in the current measurements, further delay may need to be inserted. If the delays are not matched instability could result. If delay matching cannot be ensured instability can be prevented by adding the optional low pass filters shown to the error signals Δi_d and Δi_q . These should be single-pole filters with a corner frequency of at least 5 times the system natural frequency ω_n to ensure the control loops are not affected. These filters were avoided in the experiment described in this paper by carefully matching the delays.

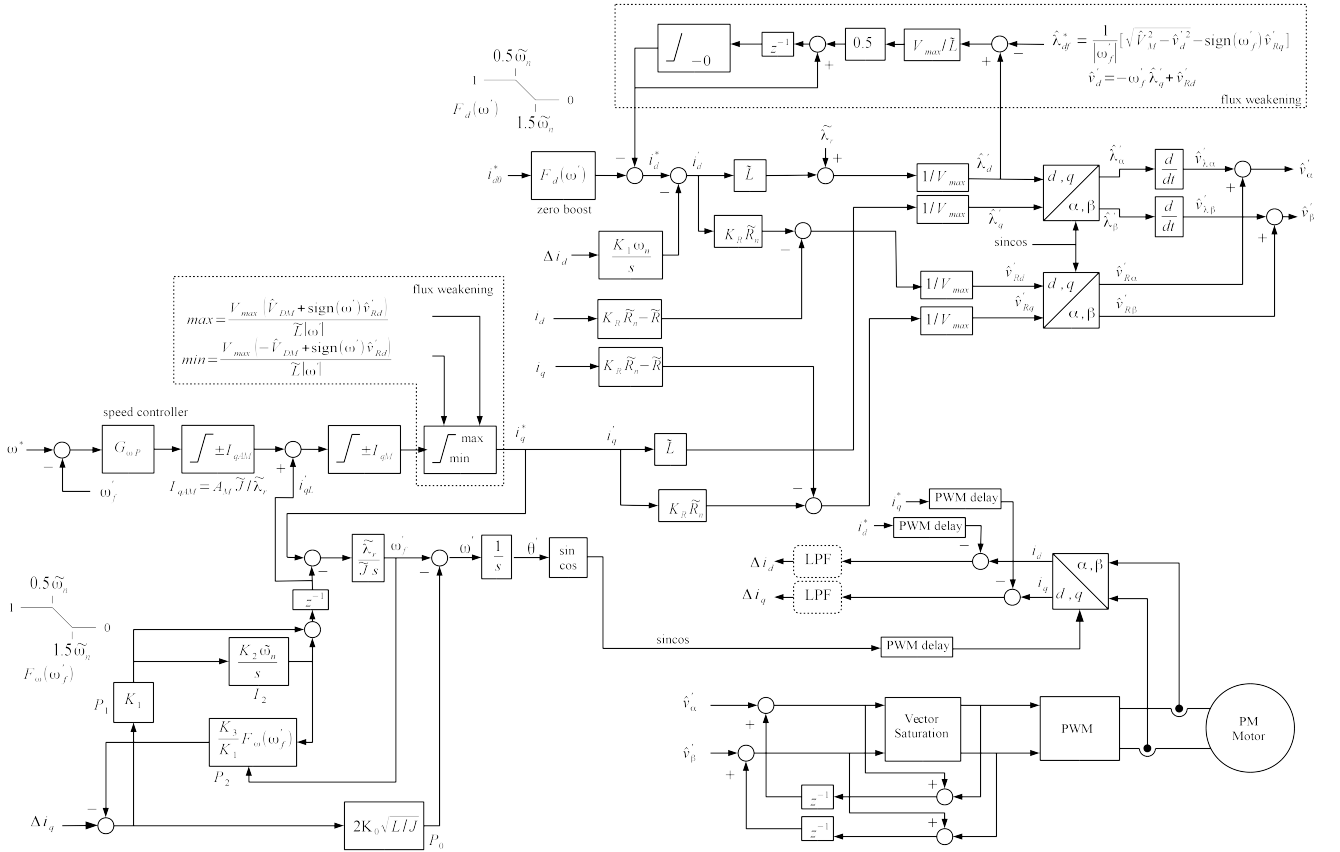


Figure 22. Block diagram of the new controller.

Not shown is the mechanism for handling severe and sudden torque overloads. If Δi_q amplitude exceeds a preset value, indicating pole slippage is about to occur, load model compensator gains are greatly increased to prevent this.

XII. EXPERIMENT

An appropriate PM motor for use with Feed Forward Torque Control is the hybrid stepper motor. The high number of poles for this machine (typically 100) allows very high resolution position control without a sensor when operating with an added position control loop. Also, for a given torque output, it has a lower volume and lower cost than other PM machines. Stepper motors are normally controlled with a rotating fixed magnitude current vector applied to the stator [17]. Its amplitude is typically set to twice the current needed to generate the required torque to ensure the motor does not drop out of synchronization, resulting in motor under-utilization or excessive motor heating. Also, steady state operation at some frequencies must be avoided to avoid resonances. Operating the stepper motor as a PM motor using FFTC avoids all these problems to produce a high performance servo like drive.

The features of FFTC are illustrated by experiment using a 100-pole NEMA 17 hybrid stepper motor. This is coupled to a DC motor to provide a load torque. Experimental data on the performance of a standard 6-pole PM motor using an earlier version of FFTC is also available in [8].

The stepper motor parameters are given in Table I with important derived parameters used in the controller given in Table II. The values of the tuning constants are those recommended in the

TABLE I
MOTOR PARAMETERS

Parameter	Value
Pole pairs	50
Phases	2
Rated current	1.68 A
Holding torque at rated current	0.44 N.m
Resistance per phase R	2.2 Ohm
Inductance per phase L	5 mH
Peak rotor flux linkage λ_r	5.0 mWebers
Motor Inertia	8E-6 kg.m ²
Motor + load inertia J	60E-6 kg.m ²

TABLE II
EQUIVALENT 2-POLE AND DERIVED PARAMETERS

Parameter	Value
Total Inertia, 2-pole equivalent	24E-9 kg.m ²
Natural resonance $\omega_n = \lambda_r / \sqrt{LJ}$	456 rad/s, 72.6 Hz
Natural resistance $R_n = \lambda_r \sqrt{L/J}$	2.28 Ohms

theoretical section of this paper. The d axis holding current at zero speed i_{d0}^* is set to 1.5A corresponding to a holding torque of 0.4 Nm..

The 50 pole-pair hybrid stepper motor is controlled using a Texas Instruments TM4C123GH6PM Arm Cortex-M4 based digital motor drive micro-controller with its PWM output driving a Texas Instruments DRV8432 dual H-bridge driver module. This module was supplied with 24VDC. Current sensing is via two Analog Devices AD8210 differential amplifiers measuring the voltages across sense resistors in each phase. The micro-controller was programmed in mixed C and assembler with the code based on the block diagram of Figure 22. The sample rate and PWM frequency is 25kHz. Speed controller calculations were processed at the reduced sample rate of 6.25kHz.

For the experiment, measurements were taken with a 4 channel analog data acquisition system with inputs from a high speed 4 channel digital to analog converter coupled to the micro-controller via a high speed serial bus. To measure the controller's phase error a 5,000 pulse per revolution incremental encoder was fitted to the motor and the measured position from this was compared with the controller's applied position. The 4 measurement channels were set to the controller's applied filtered speed, d and q axis currents and phase error.

As well as the experiment, a simulation was also undertaken using Matlab/Simulink, but the simulation results are similar to the experimental results and so are not presented here.

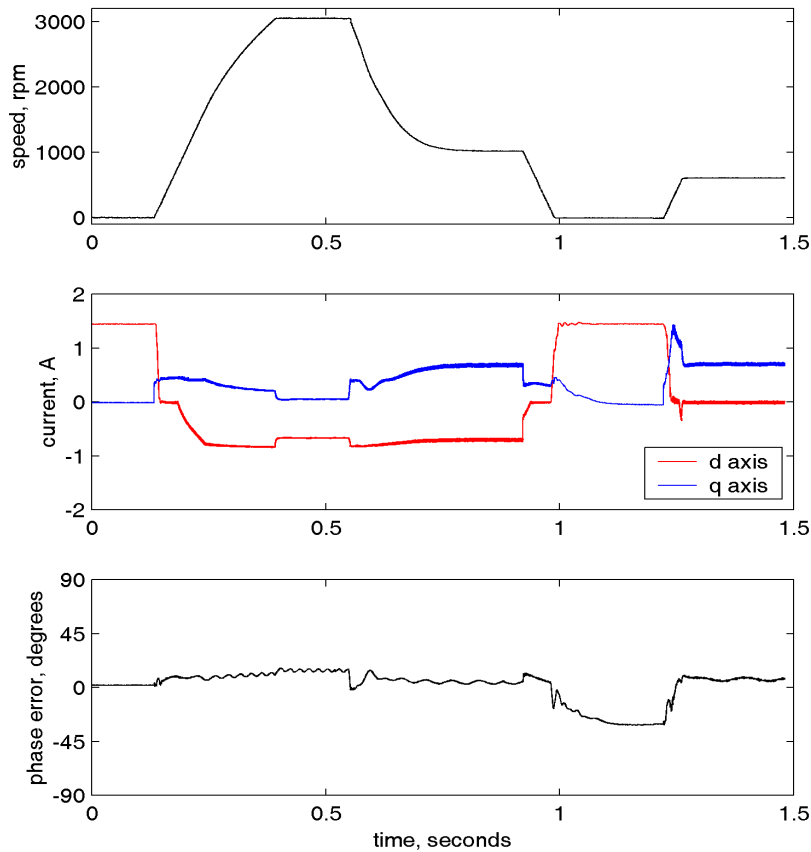


Figure 23. Experiment results for speed step to 3000 rpm at 0.15 s followed by a torque step to 0.2 Nm at 0.55 s then further speed steps to 0 and 600 rpm at 0.9 and 1.45 s.

The results are shown in Figure 23. Acceleration (and deceleration) rate is set to 15,000 rpm/sec. The motor load torque is initially set to zero. The speed is stepped to 3000 rpm at 0.15 sec. then a constant load torque of 0.2 Nm is applied at 0.55 sec. and remains for the rest of the test. The speed is then stepped to 0 at 0.9 sec then up to 600 rpm at 1.4 sec.

The initial motor rate of acceleration falls as the speed rises above 2000 rpm due to the drop in the torque limit as speed rises as per equation (18). The speed settles abruptly to the 3000 rpm set-point without over-shoot due to the high bandwidth proportional only speed control loop. The controller goes into torque limit mode immediately on the imposition of the 0.2 Nm load torque dropping the speed to 1000 rpm at which the torque limit setting has risen to match the load torque as set by equation (18). When the speed set-point drops to 0, the speed quickly drops to zero without undershoot showing the same dynamics at zero speed as at high speed even with the constant load torque of 0.2 Nm. When the speed set-point steps to 600 rpm the motor again accelerates quickly despite the load.

When not at stand-still, the phase error remains at less than 10 degrees with most of this error due to measurement delay of the encoder (indicated by the phase error increasing with speed). The high frequency ripple in the phase error was traced to run-out error in the low-cost encoder used. At zero speed with the 0.2 Nm load torque, the phase error settles to -30 degrees which is expected since the holding torque at the 1.5 A holding current is 0.4 Nm. Note the slow settling time of the phase error at zero speed under load due to the slow discharge of the integral I_2 in Figure 8 depending on the setting of the K_3 discharge constant.

Note that the d axis current drops quickly from the 1.5 A holding current set-point to zero as the speed rises without affecting speed response.

Other useful properties of the drive found from experiment include:

- 1) The motor speed can be adjusted smoothly and accurately right down to 0.1 rpm limited only by the digital resolution of the internal 16 bit speed variable.
- 2) The motor cannot be stalled, recovering quickly from a brake load. With a brake applied, the large q axis current error drives the internal speed down to near zero allowing quick synchronization once the brake is released.

More details can be found at the author's web site [18].

XIII. CONCLUSION

Described and demonstrated in this paper is a novel sensorless torque controller for the PMSM with superior performance. It is based on completely different principles to previous torque controllers. Uniquely, the controller, which uses fundamental mode only, does not use rotor position information allowing it to operate at all speeds including zero without either an external position sensor or an internal position estimator and without a change of algorithm. The new control algorithm also allows accurate and fast flux weakening to be added for operation above base speed. Even though it does not use rotor position information, it provides accurate and immediate values of load torque, rotor speed and rotor position except for a load torque dependent position error at standstill. These, together with an inherent instantaneous command torque response, allow the implementation of a fast response speed control loop using proportional control only.

REFERENCES

- [1] P. Vas, *Sensorless Vector and Direct Torque Control*, New York.: Oxford University Press, 1998.
- [2] J. Holtz and N. Oikonomou, "Fast dynamic control of medium voltage drives at very low switching frequency - an overview," *IEEE Trans. Ind. Electron.*, vol. 55, no. 3, pp. 1005-1013, Mar. 2008.
- [3] S. Vazquez, J. Rodriguez, M. Rivera, L. Franquelo, "Model predictive control for power converters and drives: advances and trends," *IEEE Trans. Ind. Electron.*, vol. 64, no. 2, pp. 935-947, Feb. 2017.
- [4] P. P. Acarnley and J. F. Watson. "Review of position-sensorless operation of brushless permanent-magnet machines," *IEEE Trans. Ind. Electron.*, vol. 53, no. 2, pp. 352-362, Apr. 2006.
- [5] M. Schroedl. "Sensorless control of AC machines at low speed and standstill based on the "INFORM" method," in *Conf. Rec. IEEE-IAS Annu. Meeting*, vol. 1, pp. 270-277, 1996.
- [6] S. Shinnaka. "A new speed-varying ellipse voltage injection method for sensorless drive of permanent-magnet synchronous motors with pole saliency—new PLL method using high-frequency current component multiplied signal," *IEEE Trans. Ind. Appl.*, vol. 44, pp. 777-788, May/June 2008.
- [7] G. Foo and M. F. Rahman. "Sensorless direct torque and flux-controlled IPM synchronous motor drive at very low speed without signal injection," *IEEE Trans. Ind. Electron.*, vol. 57, no. 1, pp. 395-403, Jan. 2010.
- [8] G. P. Hunter, "A sensorless PMSM fundamental mode controller with high dynamic full range speed control," *Proc. 37th Annu. Conf. IEEE Ind. Electron. Soc. (IECON 2011)*. 2011, pp. 1728-1733, 2011.

- [9] R. S. Colby and D. W. Novotny. "An efficiency-optimizing permanent-magnet synchronous motor drive," *IEEE Trans. Ind. Appl.*, vol. 24, no. 3, pp. 462-469, May/June 1988.
- [10] J. Itoh, N. Nomura and H. Osawa. "A comparison between v/f control and position-sensorless vector control for the permanent magnet sensorless motor," *Proc. Power Conversion Conf.*, 2002, vol.3, pp. 1310-1315, April 2002.
- [11] F. Harashima, S. Condo, K. Ohnishi, M. Kajita and M. Susono. "Multimicroprocessor-based control system for quick response induction motor drive," *IEEE Trans. Ind. Appl.*, vol. IA-21, no. 4, pp. 602-609, May/June 1985.
- [12] S. Yamamura, S. Nakagawa and A. Kawamura. "Voltage type control of induction motor by means of field acceleration method," *Electrical Engineering in Japan*, vol. 104, no. 4, pp. 89-94, 1984.
- [13] S. Bolognani, A. Faggion, L. Peretti and M. Zigliotto "Sensorless V-type vector-controlled IM drive with inherent flux-weakening capability," *Proc. 4th IET Conf. on Power Electronics, Machines and Drives*, 2008, pp. 465-469, 2008.
- [14] S. Bolognani, A. Faggion, L. Peretti and M. Zigliotto, "Parameter sensitivity analysis of two low-cost sensorless induction motor drives," *Proc. IEEE Power Electron. Specialist Conf.* 2008, pp. 43-49, 2008.
- [15] Y. Iwaji, T. Sukegawa, T. Okuyama, T. Ikimi, M. Shigyo and M. Tobise. "A new PWM method to reduce beat phenomenon in large-capacity inverters with low switching frequency," *IEEE Trans. Ind. Appl.*, vol. 35, no. 3, pp. 606-612, May/June 1999.
- [16] G. P. Hunter, "Low cost cycloconverter induction motor drives using new modulation techniques," Ph.D. thesis, Fac. Eng & I.T., Univ. Tech. Syd., Sydney, Australia, 1997.
- [17] P. Acarnley, *Stepping Motors: a guide to theory and practice*, 4th ed. Stevenage, U.K.: Inst. Elect. Eng., 2002.
- [18] G. Hunter, "Greg Hunter's Homepage" [Online], Available: <http://www.ghunter.net>